Catalysis Science & Technology

Accepted Manuscript

This article can be cited before page numbers have been issued, to do this please use: A. A. Hussein, Y. Ma and G. A. I. Moustafa, *Catal. Sci. Technol.*, 2022, DOI: 10.1039/D1CY02107A.

ROYAL SOCIETY OF CHEMISTRY

rsc.li/catalysis

View Article Online
DOI: 10.1039/D1CY02107A

ARTICLE

Predominance of the Second Cycle in the Homogeneous Os-Catalyzed Dihydroxylation: Nature of Os(VI)→Os(VIII) Reoxidation and Unprecedented Roles for the Amine-N-Oxide

Received 00th January 20xx,
Accepted 00th January 20xx

DOI: 10.1039/x0xx00000x

Aqeel A. Hussein[a]*, Yumiao Ma[b,c] and Gamal A. I. Moustafa[d,e]

The homogenous Os-catalyzed dihydroxylation of alkenes has been widely applied in organic synthesis. Mechanistic studies on the diol formation have been performed but concentrated on the osmylation step to form Os(VI) glycolate, however the details and the origin of the reactivity of the catalytic cycle that comprises several mechanistically poorly defined steps have yet to be fully understood. Here, we report density functional theory (DFT) investigations of Os-catalyzed non-enantioselective dihydroxylation of trans-butene under homogenous conditions (OsO_4/NMO) to demonstrate the predominant pathway to be through the second cycle, with reoxidation of the Os(VI) glycolate outpacing its hydrolysis. The putative Os(VIII) trioxoglycolate is found as a highly reactive intermediate that undergoes a highly rapid osmylation of another alkene, initiating the second cycle. The present study shows that tertiary amines like NMM, the oxidation coproduct, do not promote either reoxidation or hydrolysis of Os(VI) glycolate but inhibit the reaction by competing coordination. Utilizing the energetic span model on our proposed computed catalytic cycle, reoxidation of Os(VI)→Os(VIII) glycolate is found to be turnover-limiting state. The hydrolysis of Os(VI) bisglycolate, formed by the second osmylation reaction is catalyzed by NMM through a stepwise ion-pairing mechanism. In addition to the reoxidation played by NMO, it plays another role by catalyzing the hydrolysis of the stable Os(VI) bisglycolate either through the coproduct base NMM or by NMO-assisted stabilization of the stepwise ion-pairing hydrolysis of Os(VI) bisglycolate. Besides, the reoxidation step Os(VI)→Os(VIII), with and without NMM, is studied in detail by combining localized and principle interacting orbital and distortion/interaction analysis. The findings presented in this work will encourage experimentalists to implement further studies on Os catalysis to design a more efficient catalytic version that tackles enantioselective deficiencies in the 1,2-diol formation and even in oxidative cyclization of 1,5-dienes to give tetrahydrofuran diols.

Introduction

Vicinal diols are valuable intermediates in numerous syntheses and this moiety is present in many naturally occurring and synthetic bioactive molecules.[1,2] *syn*-Dihydroxylation of alkenes catalyzed by osmium tetroxide is probably the most widely applied method used to access 1,2-diols, certainly on a laboratory scale, and particularly where stereochemically defined products are sought (Figure 1a).[1,2] However, due to high toxicity, volatility, and high cost of OsO_4, recent interests are turned to more environmently-friendly protocols, where Os-free asymmetric *syn*-dihydroxylations have been developed in the last two decades.[3] Secondary oxidizing agents (SOA) including *tert*-butylhydroperoxide (TBHP),[4] amine *N*-oxides (e.g. *N*-methylmorpholine *N*-oxide, NMO),[5] or potassium hexacyanoferrate(III) ($K_3Fe(CN)_6$)[6] have been employed for reoxidation of Os (VI) species during catalysis. Two of the best known methods of catalytic dihydroxylation are the Upjohn (OsO_4/NMO)[5a,b] and Sharpless asymmetric dihydroxylation ($K_3Fe(CN)_6/K_2CO_3$; SAD) protocols,[1a,2,5c,6b] the latter exploiting cinchona alkaloid-derived ligands to achieve enantioselectivity. Mechanistically, addition of OsO_4 to alkenes proceeds by (3+2) cycloaddition, with an alternative proposal involving a (2+2) pathway having been excluded based on combination of theoretical and kinetic isotope effect studies.[7]

While calculations delivered valuable insights into the mechanism of alkene osmylation, there remains a dearth of computational study of other important aspects integral to catalytic dihydroxylation, including all ensuing reactions of the resulting Os(VI) glycolates. A second catalytic cycle, also giving rise to diols, was identified in dihydroxylation where the SOA and Os are in the same phase (Figure 1b).[8–10] It was proposed that oxidation of Os(VI) glycolate intermediate **3** by the SOA gives an Os(VIII) trioxoglycolate **4** that may osmylate another olefin substrate through this so-called second cycle. In the context of SAD, the second cycle is deleterious to enantioselectivity, particularly for more substituted olefins

[a] Department of Pharmacy, College of Medicine, Komar University of Science and Technology, Sulaymaniyah, Kurdistan Region, Iraq; orcid.org/0000-0002-9259-9609; Email: aqeel.alaa@komar.edu.iq
[b] BSJ Institue, Haidian, Beijing, 100084, People's Republic of China.
[c] Hangzhou Yanqu Information Technology Co., Ltd. Xixi Legu Creative Pioneering Park, No. 712 Wen'er West Road, Xihu District, Hangzhou City, Zhejiang Province, 310003, People's Republic of China.
[d] Department of Medicinal Chemistry, Faculty of Pharmacy, Minia University, Minia 61519, Egypt.
[e] Department of Chemistry, University of Southampton, Southampton, Hampshire, SO17 1BJ, UK.

Electronic Supplementary Information (ESI) available: Additional calculated structures, cartesian coordinates, absolute energies for reported structures. See DOI: 10.1039/x0xx00000x

View Article Online
DOI: 10.1039/D1CY02107A

where Os glycolate hydrolysis is sluggish.[8] Therefore, modifications that minimised the second cycle were developed, including slow addition of the olefin,[8] introduction of additives,[9] or by using a basic *t*-BuOH/H_2O system where osmylation and reoxidation of Os(VI) proceed in different phases.[6b]

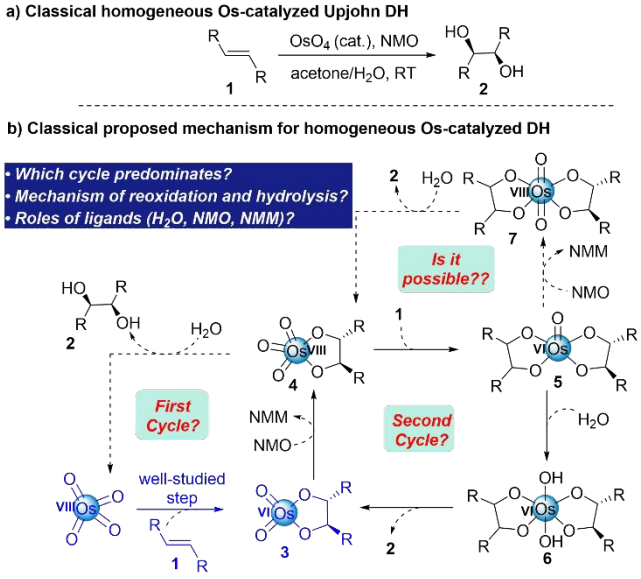

Fig. 1. a) Dihydroxylation (DH) of alkenes under classical homogenous conditions (OsO_4/NMO). b) The classical proposed mechanism for Os-catalysed DH showing two proposed catalytic cycles.[10]

The presence of Os(VIII) trioxoglycolates **4** as intermediates at the intersection of the two cycles is widely accepted; their existence is inferred from observation of the second cycle,[8–10] and formation of Os(VI) bisglycolates.[11] However, Os(VIII) trioxoglycolates **4** have not been isolated or characterized. Despite the many experimental studies focused on this cornerstone reaction but steps of producing 1,2-diol moiety are still not clearly judged. To date, most of computational investigations have been mainly focused on the osmylation step of the reaction, either with or without ligands.[7] However, no in-depth theoretical examination has appeared in literature to tackle the omniphilic mechanistic pathway since the catalytic cycle comprises several mechanistically poorly defined steps, including reoxidation of Os(VI) to Os(VIII) in glycolate intermediates, hydrolysis of Os(VI) or Os(VIII) glycolates and competition of the first and the second cycles as well as effect of the coproduct amine on reoxidation and hydrolysis. Here, we report a density functional theory (DFT) study of these reaction steps for a representative *trans*-disubstituted alkene, (*E*)-but-2-ene (**8**),[12] finding the Os(VIII) trioxoglycolate as an unstable intermediate, which readily engages in osmylation of another olefin molecule. The findings are consistent with the predominance of second cycle osmylation under Upjohn dihydroxylation conditions and shed light on why Os(VIII) trioxoglycolates have not been observed as isolable species. In addition, despite the main role for the SOA, amine-N-oxides, NMO, is reoxidation (Os(VI)→Os(VIII)), the results demonstrate that the SOA plays another dual role through providing the coproduct NMM, after reoxidation, as a base, to catalyze the hydrolysis of the Os(VI) bisglycolate **17** and stabilizing the stepwise hydrolysis of **17** as a ligand (NMO).

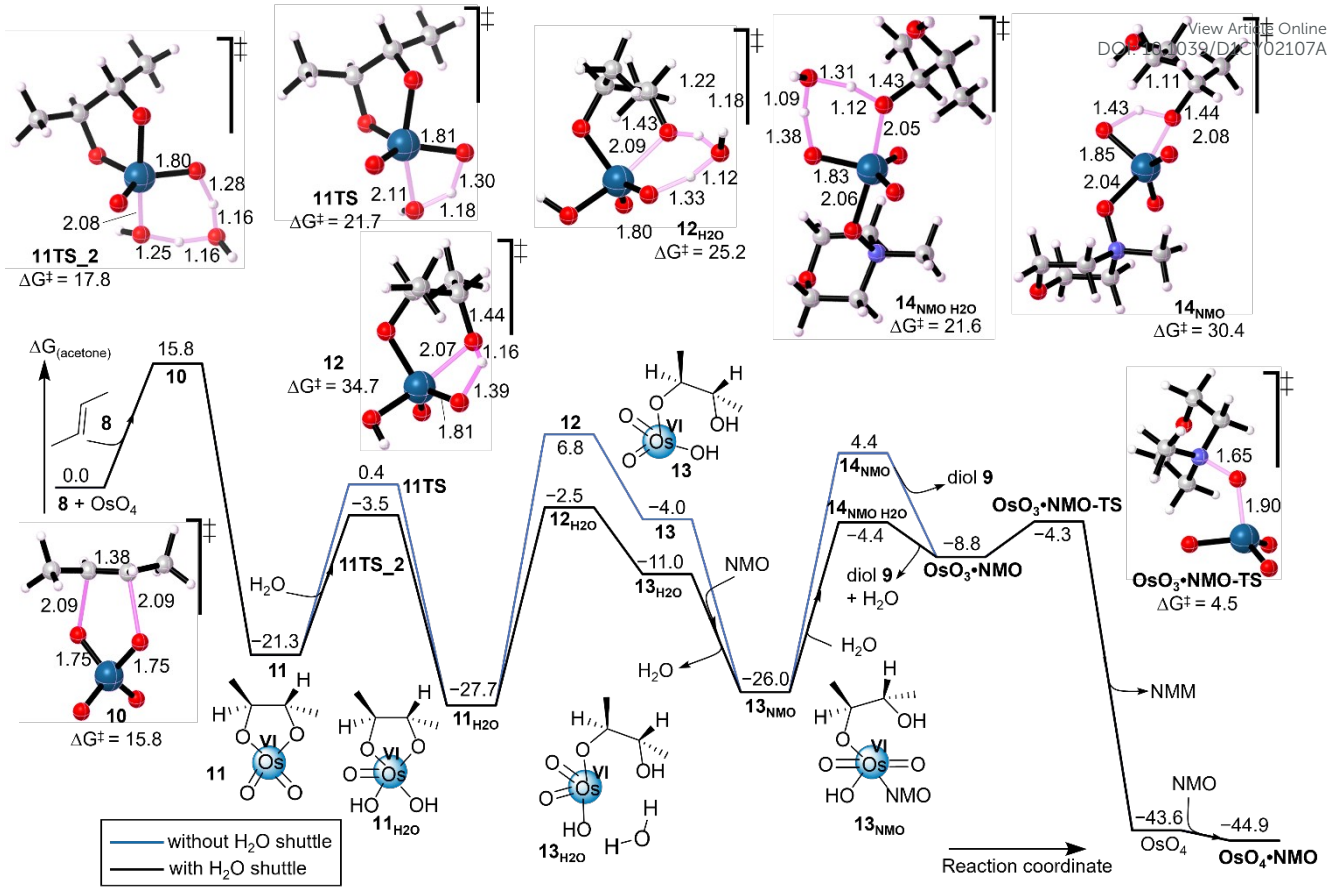

Fig. 2. Formation of Os(VI) dioxoglycolate **11** followed by disfavorable ligand-naked Os(VI) hydrolysis calculated by the SMD-(acetone)-M06/6-311+G(d,p),def2-TZVP//M06/6-31G(d),LANL2DZ level of theory at 298.15 K. Bond lengths in angstrom and energies in kcal/mol.

Results and Discussions

Initial considerations. Dihydroxylation of alkene **8** to give (2*R**,3*R**)-butane-2,3-diol (**9**) was investigated with DFT simulations using the optimization protocol performed with the (SMD)-M06/6-311+G(d,p),def2-TZVP level of theory in acetone as solvent medium based on gas phase optimized geometries performed with the M06/6-31G(d),LANL2DZ level of theory.[13] The alkene osmylation step has previously been studied using DFT calculations,[7] and interest here lies primarily in subsequent steps that give rise to diol product and Os species capable of propagating catalysis. Of many pathways available to the initially formed Os(VI) dioxoglycolate intermediate, the present study considers addition of ligands (H_2O, NMM and NMO), hydrolysis, reoxidation (Os(VI)→Os(VIII)), in the first and second cycles.[14]

Reaction mechanism of the simplest pathway for diol formation via hydrolysis of Os(VI) glycolate. Osmylation of alkene **8** by OsO_4 proceeds through (3+2) cycloaddition TS **10** with a barrier of 15.8 kcal/mol (Figure 2), giving tetrahedral Os(VI) dioxoglycolate **11** as an exergonic step (ΔG_{osm} = −21.3 kcal/mol).[7,13,15] It is important to mention here that based on our previous computations [12] and literature reported by Strassner,[7j] the triplet state of the Os(VI) glycolate is energetically disfavored compared to singlet spin multiplicity and thus triplet state was excluded. Following formation of Os(VI) dioxoglycolate **11**, different pathways can give rise to vicinal diol **9**; direct hydrolysis of Os(VI) dioxoglycolate **11** was examined first. Insertion of a water molecule is exergonic of 6.4 kcal/mol to form hydrated Os(VI) intermediate $\mathbf{11_{H2O}}$ with a barrier of 17.8 kcal/mol via a six-membered ring TS **11TS_2** (shuttled by H_2O) and 21.7 kcal/mol via four-membered TS **11TS** (non-shuttled). Calculations show hydrolysis of Os(VI) glycolate **11** following an associative pathway, as an endergonic process that requires substantial barriers to be overcome via four-membered ring transition state (TSs) (TSs **12** and $\mathbf{14_{NMO}}$; $\Delta G^{‡}$ = 34.5 kcal/mol and 30.4 kcal/mol, respectively), indicating a disfavorable hydrolysis. In this context, introducing another water molecule in the hydrolysis TSs **12** and $\mathbf{14_{NMO}}$ led to lower barriers to 25.2 and 21.6 kcal/mol, respectively, for the less strained six-membered ring TSs $\mathbf{12_{H2O}}$ and $\mathbf{14_{NMO\ H2O}}$. Here, the second water molecule behaves as a shuttle to facilitate the transfer of the proton during glycolate opening. The ring-opened Os glycolate intermediate $\mathbf{13_{H2O}}$ is a relatively unstable species, stabilised following coordination of NMO to give $\mathbf{13_{NMO}}$. Release of the glycol **9** is catalyzed by a water molecule shuttle, exhibiting a reduced barrier of 21.6 kcal/mol compared to 30.4 kcal/mol when the additional H_2O molecule is absent. The results are consistent with slow hydrolysis of Os(VI) glycolates under neutral conditions and favorable coordination of the diol to

Os(VI) (see SI1).[14b,16] In this regard, the experimental activation energy (E_a^{exp}) for hydrolysis of osmate ester of 3-cyclohexenecarboxylic acid was reported to be 19.0 kcal/mol whereas the calculated one for *trans*-2-butene **8** (E_a^{calc}) is 17.8 kcal/mol, providing confidence in the chosen level of theory.[14a] To close the first cycle, reoxidation of the hydrolysed Os(VI) species by NMO to reform OsO_4 was considered as two elementary steps, namely NMO complexation and oxo-transfer,[17,18] and found to be thermodynamically favored. OsO_4 arises from oxo-transfer within the complex OsO_3•NMO with a low barrier of 4.5 kcal/mol as a thermodynamically exergonic step. Association of NMO to OsO_4 is close to thermoneutral (ΔG = −1.3 kcal/mol).[19,20] We therefore conclude that the hydrolysis pathway via Os(VI) glycolate is slow with the current conditions because of the barriers needed along TS **12$_{H2O}$** and **14$_{NMO.H2O}$** and consequently the pathway is not favored in comparison to reoxidation of Os(VI) glycolate (see below in Figure 3). However, the calculated energies of Os(VI) hydrolysis shown in Figure 2 are clearly consistent with slow hydrolysis of Os(VI) glycolates under neutral conditions and favourable coordination of the diol to Os(VI) (see also Figure SI1).[14b,16]

Reoxidation of Os(VI) to Os(VIII) glycolate and diol formation via hydrolysis of Os(VIII) glycolate *vs* second cycle. A second important reaction manifold available to the Os(VI) dioxoglycolate **11** is reoxidation by NMO to give Os(VIII) trioxoglycolate **11$_{[ox]}$**, with ensuing hydrolysis or osmylation through the second cycle (Figure 3, right-hand pathway). Coordination of NMO to Os(VI) glycolate **11** gives a stable complex of pentacoordinate Os(VI) species **11$_{NMO}$** (ΔG = −10.4 kcal/mol) which undergoes an oxo-transfer process through a relatively low barrier of 12.2 kcal/mol to give the trioxoglycolate **11$_{[ox]}$** as a thermoneutral step with release of NMM.[21] Osmylation of a second alkene molecule by **11$_{[ox]}$** was found to be highly favorable thermodynamically (ΔG_{osm} = −52.7 kcal/mol) and proceeding as a near-barrierless process ($\Delta G^{\ddagger}$ = 0.6 kcal/mol), through TS **16** to give distorted square-pyramidal Os(VI) oxobisglycolate **17**.[22] The extremely low-barrier and near-barrierless nature of **16** is further validated by a series of

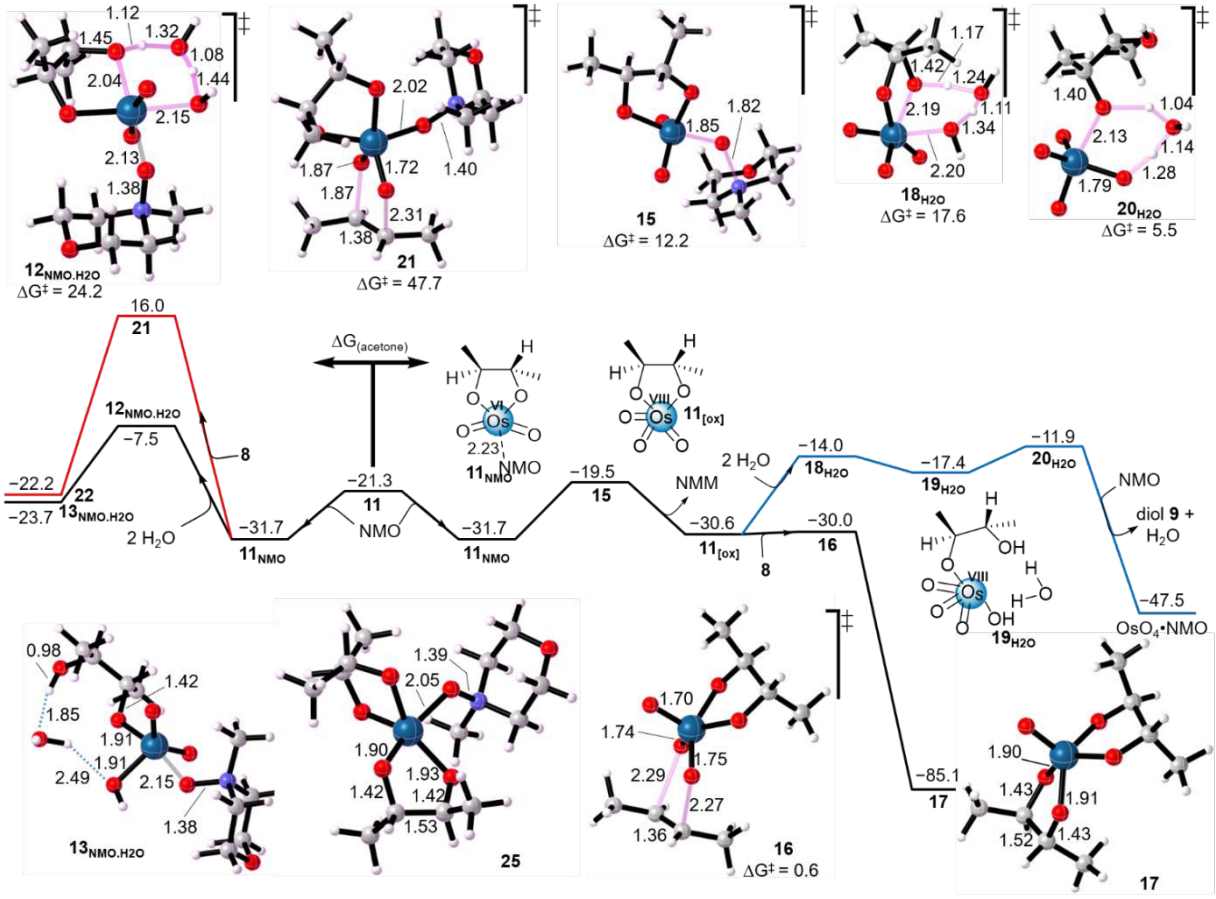

Fig. 3. Reoxidation of Os(VI)→Os(VIII) glycolate followed by competition between hydrolysis and intermolecular osmylation (right) compared with hydrolysis and intermolecular osmylation of NMO-complexed Os(VI) **11$_{NMO}$** (left), calculated by the SMD-(acetone)-M06/6-311+G(d,p),def2-TZVP//M06/6-31G(d),LANL2DZ level of theory at 298.15 K. Bond lengths in angstrom and energies in kcal/mol.

View Article Online
DOI: 10.1039/D1CY02107A

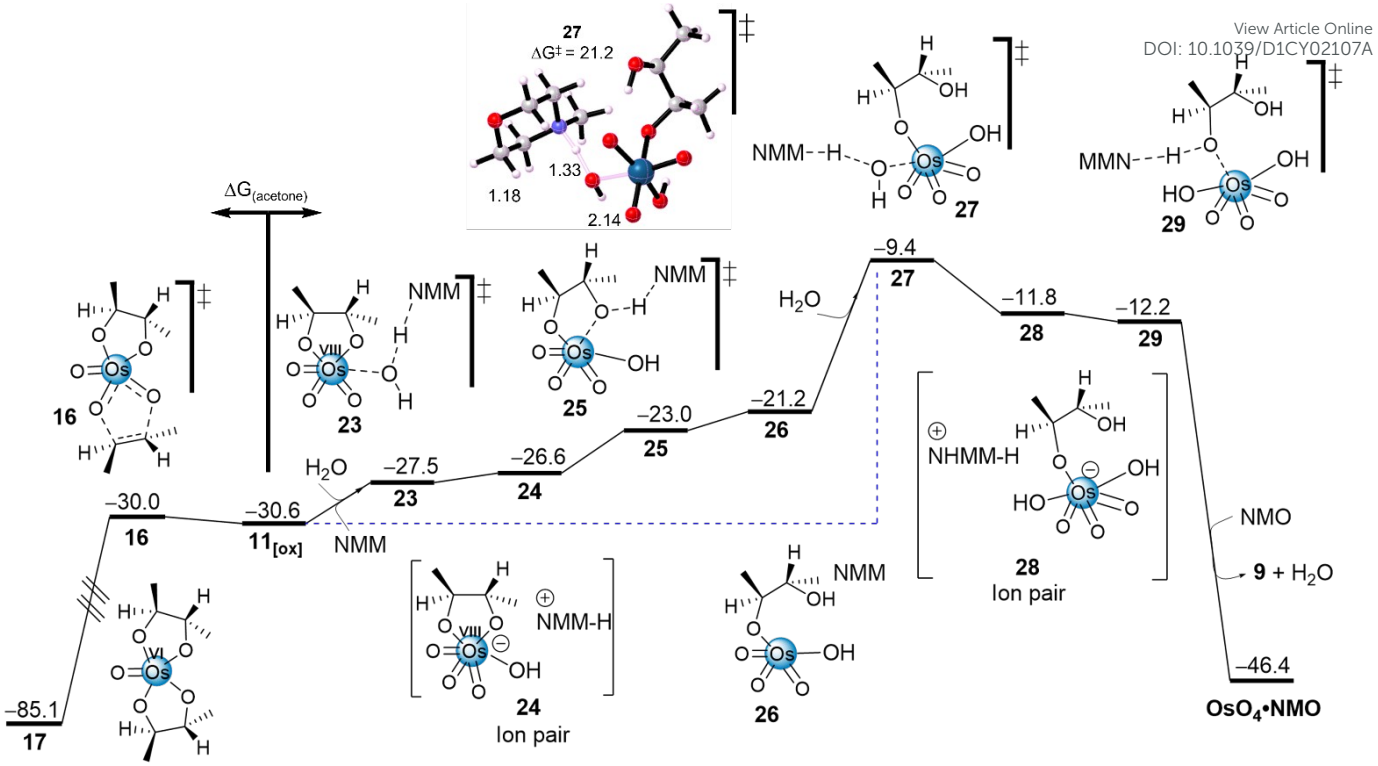

Fig. 4. Mechanism of amine (NMM)-assisted hydrolysis of Os(VIII) trioxoglycolate $\mathbf{11_{[ox]}}$ to release diol **9** and regenerate OsO_4•NMO through the first cycle calculated by the SMD-(acetone)-M06/6-311+G(d,p),def2-TZVP//M06/6-31G(d),LANL2DZ level of theory at 298.15 K. Bond lengths in angstrom and energies in kcal/mol.

different functionals and basis sets, as shown in Table SI1. To gain further understanding of the barrierless of TS **16**, we calculated the interaction energy between $\mathbf{11_{[ox]}}$ and alkene **8** from Distortion/Interaction analysis. The result indicates a highly favorable interaction energy of −11.4 kcal/mol, as compared to the negligible distortion energy of 1.7 kcal/mol, subsequently reducing the barrier during the intermolecular (3+2) cycloaddition. By contrast, hydrolysis of Os(VIII) trioxoglycolate $\mathbf{11_{[ox]}}$ requires comparatively higher energy barrier through TS $\mathbf{18_{H2O}}$ ($\Delta G^{\ddagger}$ = 16.6 kcal/mol) to give unstable intermediate $\mathbf{19_{H2O}}$ (ΔG = 13.2 kcal/mol) and the latter needs further barrier of 5.5 kcal/mol via TS $\mathbf{20_{H2O}}$ to be surmounted to release OsO_4•NMO and diol **9** (Figure 3, blue right-hand pathway). However, the backward reaction for $\mathbf{19_{H2O}}$ during the hydrolysis of $\mathbf{11_{[ox]}}$ is kinetically faster through TS $\mathbf{18_{H2O}}$ than the forward step through TS $\mathbf{20_{H2O}}$.

Given the favored calculated energy of the Os(VIII) trioxoglycolate formation, we also considered whether the second cycle, or indeed hydrolysis, might proceed by way of an alternative intermediate such as NMO-complexed Os(VI) glycolate $\mathbf{11_{NMO}}$. The reactions of NMO-complexed Os(VI) intermediate $\mathbf{11_{NMO}}$ with water (hydrolysis) and with *E*-but-2-ene were therefore considered (Figure 3, left). Intermolecular osmylation of *E*-but-2-ene by $\mathbf{11_{NMO}}$ was calculated to be thermodynamically disfavored (NMO-complexed bisglycolate Os(IV) intermediate **22**, ΔG_{osm} = 9.5 kcal/mol) with a substantially high barrier via TS **21** ($\Delta G^{\ddagger}$ = 47.7 kcal/mol). Hydrolysis of $\mathbf{11_{NMO}}$ is also found to have a high barrier via six-membered ring TS $\mathbf{12_{NMO.H2O}}$ ($\Delta G^{\ddagger}$ = 24.2 kcal/mol) leading to an endergonic intermediate $\mathbf{13_{NMO.H2O}}$ (ΔG = 8.0 kcal/mol). These alternative pathways should therefore not compete with reoxidation of **11** to trioxoglycolate $\mathbf{11_{[ox]}}$ that subsequently enters the second cycle as a favored pathway.

Furthermore, inclusion of NMM as a base did not lower the barrier of hydrolysis for the Os(VIII) trioxoglycolate $\mathbf{11_{[ox]}}$ compared to reoxidation (Figure 4). NMM indeed promotes the hydrolysis due to its basicity, but it is found to be a stepwise process in every single glycolate bond hydrolysis. Initially, the first glycolate hydrolysis is found to be an endergonic process with the intermediates being located higher in energy than its TS due to the intrinsically low barrier. However, the second glycolate bond requires a barrier of 21.2 kcal/mol through TS **27** kcal/mol to release the ion pair intermediate **28** that followed by a barrierless step to furnish the diol **9** and regenerate OsO_4•NMO. It is noticed that TSs are often lower in energy than the corresponding intermediates. This is because the minimum of these intermediates is too shallow on the potential energy surface by which intrinsic reaction coordinate calculations showed that these intermediates are very close in energy to the TSs, and thus the corrections on vibration and entropy lead to the lower TS energy. Although the above-mentioned calculations were performed by geometry optimization in gas phase, it is shown that re-optimization under implicit solvation of acetone leads to only very negligible change on the energetics, as shown in the Supporting Information.

View Article Online
DOI: 10.1039/D1CY02107A

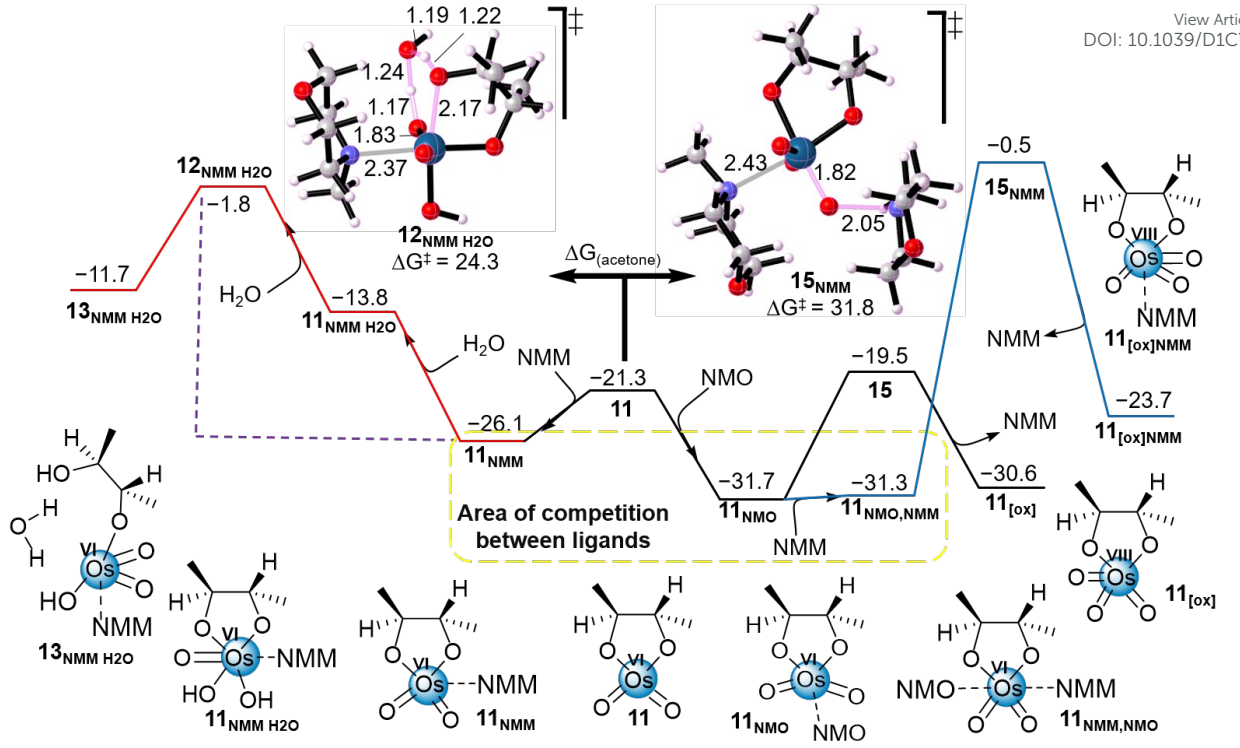

Figure 5. Effect of amine NMM on reoxidation (Os(VI)→Os(VIII)) and hydrolysis of Os(VI) glycolate **11** and compared with reoxidation in the absence of NMM, calculated by the SMD-(acetone)-M06/6-311+G(d,p),def2-TZVP//M06/6-31G(d),LANL2DZ level of theory at 298.15 K. Bond lengths in angstrom and energies in kcal/mol.

Effect of tertiary amine (NMM) on reoxidation (Os(VI)→Os(VIII)) and hydrolysis of Os(VI) glycolate 11. The influence of NMM, present as the coproduct of reoxidation, was also considered for the oxo-transfer process within Os-NMO complexes and hydrolysis of Os(VI) **11** (Figure 5). Coordination of NMM to $\mathbf{11}_{\mathbf{NMO}}$ is nearly thermoneutral (ΔG = 0.4 kcal/mol), but the resulting complex $\mathbf{11}_{\mathbf{NMO,NMM}}$ requires a substantial barrier of $\Delta G^{\ddagger}$ = 31.8 kcal/mol to progress the oxo-transfer from N to Os as indicated in TS $\mathbf{15}_{\mathbf{NMM}}$ (Figure 5, right). In contrast, the oxo-transfer requires a slightly lower barrier of 12.2 kcal/mol in the absence of NMM, so NMM is unlikely to be involved in the reoxidation. The increased barrier from $\mathbf{11}_{\mathbf{NMO,NMM}}$ compared to reoxidation from $\mathbf{11}_{\mathbf{NMO}}$ will be discussed in the later part (see below). Importantly, addition of tertiary amine like NMM to the square pyramidal Os(VIII) trioxoglycolate, forming octahedral Os(VIII) trioxoglycolate $\mathbf{11}_{\mathbf{[ox]NMM}}$, is thermodynamically endergonic of ~7.0 kcal/mol. Pyridine and other amines previously showed to retard the rate of catalytic dihydroxylation of alkenes, and this has been attributed to the reoxidation step.[21] Furthermore, the involvement of NMM as a ligand during hydrolysis of Os(VI) glycolate **11** was also found to be unlikely compared to reoxidation step (Figure 5, left). Despite favorable coordination of NMM to **11** (ΔG = –4.8 kcal/mol), which is less exergonic than complexation with NMO (ΔG = –10.4 kcal/mol), hydrolysis of the resulting NMM-complexed Os(VI) $\mathbf{11}_{\mathbf{NMM}}$ is disfavored due to a relatively high barrier of 24.3 kcal/mol *via* six-membered TS $\mathbf{12}_{\mathbf{NMM\ H2O}}$ as an endergonic step. A further supportive finding that prevents hydrolysis of $\mathbf{11}_{\mathbf{NMM}}$ and prefers reoxidation is that coordination of $\mathbf{11}_{\mathbf{NMM}}$ with NMO is modestly exergonic of 2.4 kcal/mol. It was reported that ligands such as pyridine or others stabilize the Os(VI) glycolete towards hydrolysis.[23] This would clearly envision us that any Os(VI) glycolate liganded with an amine spontaneously shifts to complexation with an amine-N-oxide when it is homogenously conditioned to subsequently furnish Os(VIII) trioxoglycolate $\mathbf{11}_{\mathbf{[ox]}}$.[24]

Reoxidation of Os(VI) dioxoglycolate **11** to give Os(VIII) trioxoglycolate $\mathbf{11}_{\mathbf{[ox]}}$ is comparatively favorable over hydrolysis under neutral conditions, and alkene osmylation by $\mathbf{11}_{\mathbf{[ox]}}$ is highly exergonic and has a modest barrier.[21] Therefore, the second cycle should outpace hydrolysis of Os(VIII) $\mathbf{11}_{\mathbf{[ox]}}$ or hydrolysis of Os(VI) **11** under typical Upjohn or homogenous conditions. The very high reactivity of $\mathbf{11}_{\mathbf{[ox]}}$ towards osmylation through the second cycle may be reconciled with the absence of reported examples where Os(VIII) trioxoglycolates have been isolated or characterized.

Orbital nature of the reoxidation reaction and the influence of NMM. To reveal the nature of interaction between the Os center and NMO during the oxygen-atom-transfer (OAT) process ($\mathbf{11}_{\mathbf{NMO}}$→$\mathbf{11}_{\mathbf{ox}}$ or $\mathbf{11}_{\mathbf{NMO.NMM}}$→$\mathbf{11}_{\mathbf{ox}}$), a total of 68 points were extracted from intrinsic reaction coordinate (IRC) of the transition state **15** or $\mathbf{15}_{\mathbf{NMM}}$ (Figure 6b). Analysis was carried out using Mayer's bond order,[25] and Pipek-Mezey localized orbital,[26] a robust orbital localization method especially suitable

View Article Online
DOI: 10.1039/D1CY02107A

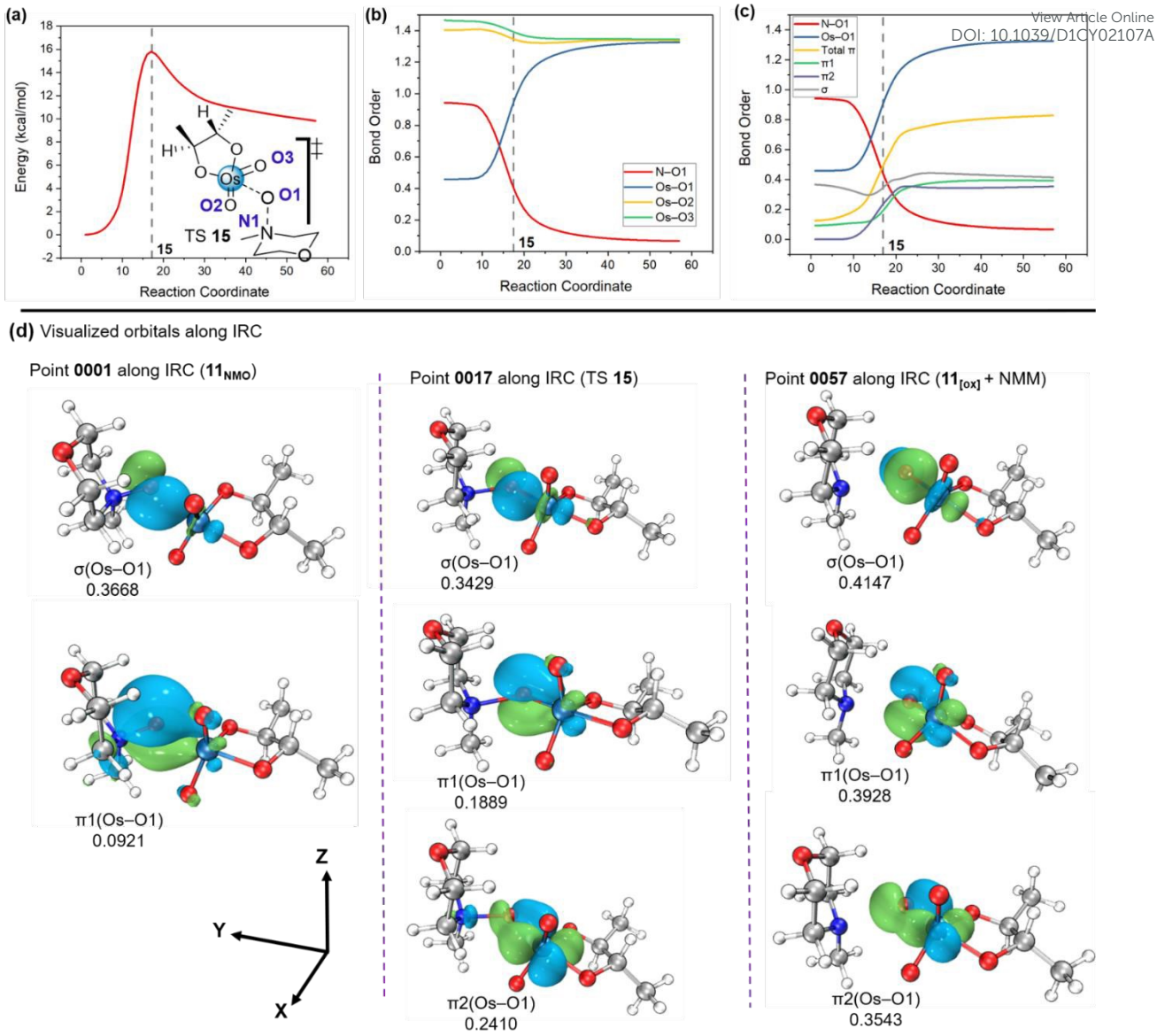

Figure 6. Effect of amine NMM on reoxidation (Os(VI)→Os(VIII)) and hydrolysis of Os(VI) glycolate **11** and compared with reoxidation in the absence of NMM, calculated by the SMD-(acetone)-M06/6-311+G(d,p),def2-TZVP//M06/6-31G(d),LANL2DZ level of theory at 298.15 K. Bond lengths in angstrom and energies in kcal/mol.

for compounds with complex electronic structure. For $\mathbf{11}_{\mathbf{NMO}}$, the Os–O1 bond order is determined to be 0.3347, indicating a weak but still significant covalent interaction. The presence of covalent bonding is further proved by the localized orbital found between Os and O1, corresponding to an Os–O1 σ bond. As shown in the bond order curve along the IRC pathway of TS **15**, the Os–O1 bond order rises sharply to ~1.3 upon the OAT reaction, in a synchronous manner with respect to the cleavage of the N–O bond, where bond order decreases from 0.9596 to 0.4358 for **15**, and to zero after OAT completes.

The Os–O1 bond order is further decomposed to different type of bonding (Figures 6c and 6d). The strength of σ(Os–O1) changes only slightly along the IRC. In addition, new π(Os–O1) interactions appear during the OAT process. Although a localized orbital with π(Os–O1) character also exists at the beginning of the IRC path, it is very close to the pure p orbital of O1 atom and contributes minimally to the total Os–O1 bonding.

For TS **15**, this π bonding orbital, namely π1(Os–O1), becomes rather significant as it is formed by the O1 p orbital perpendicular to the xy plane and the Os dyz orbital. In the meantime, another localized orbital with π character, namely π2(Os–O1), formed by an in-plane oxygen p orbital along the N–O1 direction and the Os dxy orbital is also developing in a synchronous manner with π1(Os–O1). Overall, two different types of π bonding are developed during the OAT reaction, while the σ bonding is almost unchanged. The change in bonding mode finally affords a total Os–O1 bond order at ~1.3, to which two types of π bonding and one σ bond each contributes 1/3 of it.

View Article Online
DOI: 10.1039/D1CY02107A

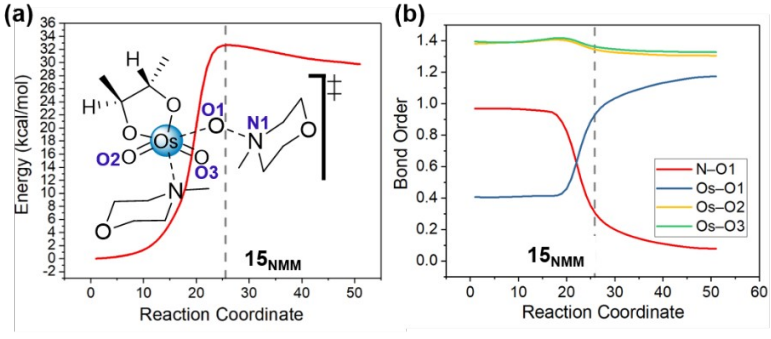

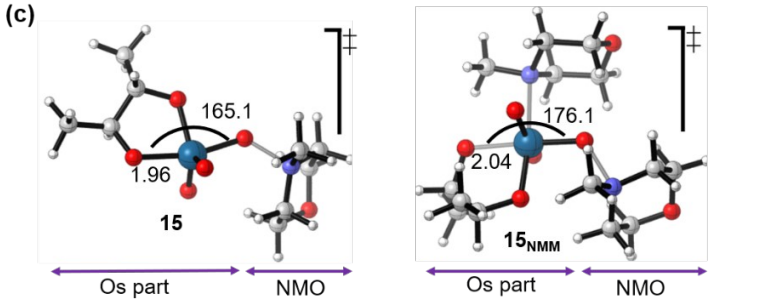

Compound	Distortion Energy for Os(VI) part	Distortion Energy for NMO	Interaction Energy
11$_{NMO}$	8.8	0.7	–32.2
15	18.2	31.5	–57.3
11$_{NMO.NMM}$	10.8	0.9	–31.1
15$_{NMM}$	32.0	51.8	–69.6

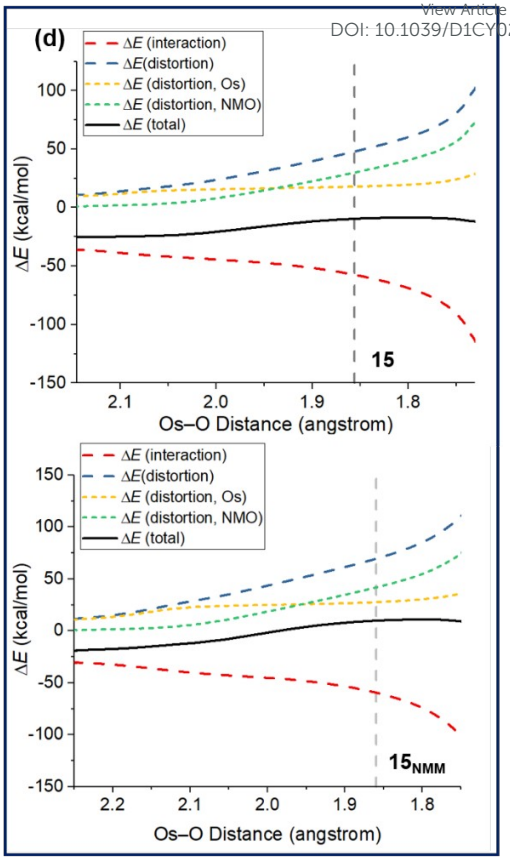

Figure 7. (a) The energy profile for the OAT reaction with **15**$_{NMM}$ along the IRC. (b) The evaluation of key bond orders along the IRC path of **15**$_{NMM}$. (c) The distortion/interaction analysis results (in kcal/mol) of TSs **15**$_{NMM}$ and **15** and their corresponding reactants **11**$_{NMO}$ and **11**$_{NMO.NMM}$, where bong lengths in angstrom and angles in degree. (d) The distortion/interaction energies of TSs **15** and **15**$_{NMM}$ along potential energy surface of IRC.

It is worth noting that the transition state **15**$_{NMM}$ has a very high energy compared to its analogue without an extra NMM ligand, namely **15**, which renders the reoxidation of **11**$_{NMM}$ rather unfavorable. In order to find out the reason why NMM ligand affects the barrier to such a large extent, the evaluation of key bond orders was examined along the IRC pathway (Figure 7a,b). Interestingly, although the energy profile indeed exhibits an electronic barrier of ~32 kcal/mol, much higher than the value of ~16 kcal/mol for **15**, the two bond order curves are quite similar. The strong similarity prompted us to conduct a more detailed analysis by distortion/interaction analysis [27] and principle interacting orbital (PIO) methods.[28] Further examination on the geometry of **15**$_{NMM}$ and **15** shows that **15**$_{NMM}$ bears a significantly longer Os–O bond (2.04 Å, compared to 1.96 Å in **15**) trans to the incoming NMO compared to **15**. As a result, we propose that the destabilization of **15**$_{NMM}$ originates partly from the weakened Os–alkoxyl group interaction, which could be attributed to the trans-influence [29] of the forming Os–O multiple bonding. In the presence of NMM ligand, the O(trans)–Os–O(NMO) forms a better linear alignment than **15**, which maximizes the trans-influence. It is also noteworthy that the N–O bond in the NMO part differs significantly (1.83 Å for **15** and 2.04 Å for **15**$_{NMM}$). This effect of these geometrical changes was explored by distortion-interaction analysis (Figure 7c,d).

In this analysis, **15**, **15**$_{NMM}$ and their corresponding starting species, namely **11**$_{NMO}$ and **11**$_{NMO.NMM}$, were divided into two fragments: the incoming NMO, and the rest (named as Os part). The energy of both the two parts were compared to that for the fully optimized minimums, and the difference was the distortion energy of each fragment (Figure 7c). The interaction energy of the two fragments was defined by the difference of the energies for the full molecule and the sum of two fragments. According to the results, it is clear that the presence of NMM has negligible effect on **11**$_{NMO}$ (versus **11**$_{NMO.NMM}$) but leads to large distortion to both Os and NMO part in **15**$_{NMM}$. The huge increase in these two terms is in agreement with the elongated Os–O(trans) and N–O bond in **15**$_{NMM}$ respectively. On the other hand, the increase in interaction energy could not outcompete the unfavorable distortion energy, leading to overall destabilization.

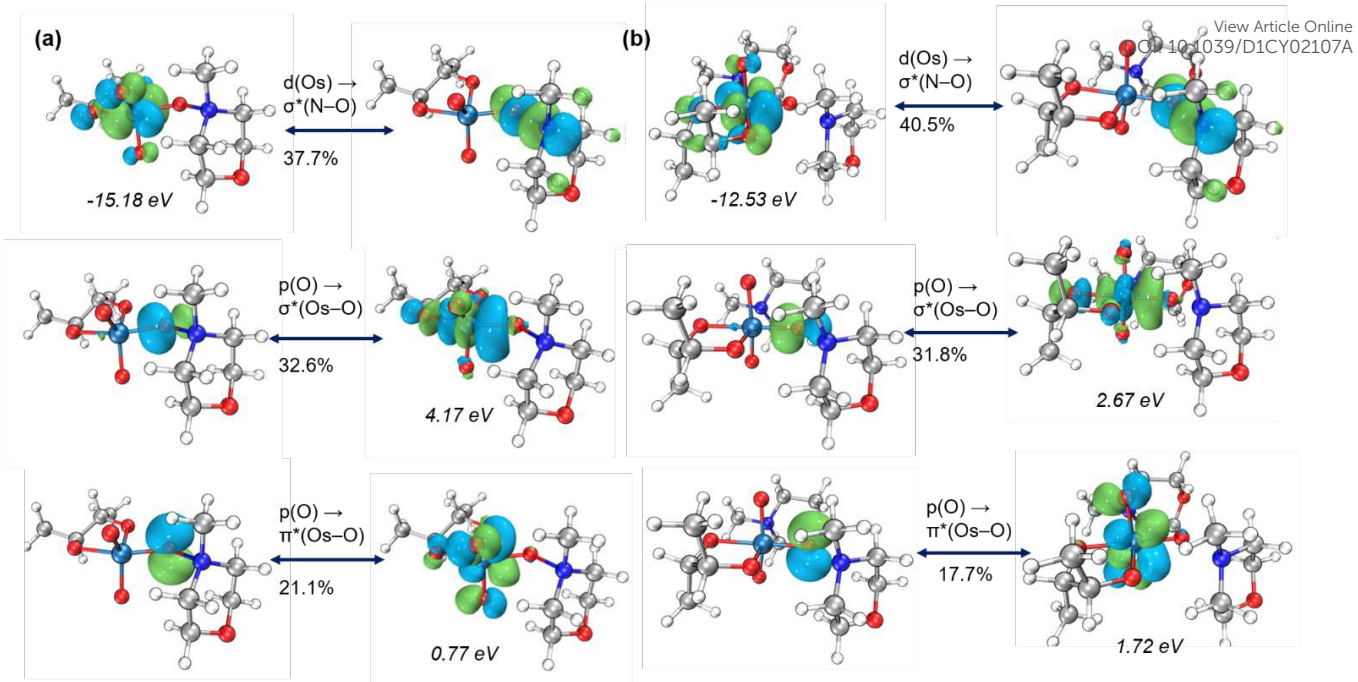

Fig. 8. PIO paired orbitals and the contribution percent (%) to the total interaction for **15** (a) and **15**$_{NMM}$ (b). Energy levels for the corresponding localized orbital related to the Os part in **11**$_{NMO}$ and **11**$_{NMO.NMM}$ are shown in italic style.

To further reveal the orbital nature of the Os–NMO interaction and the reason of the changes in geometry and interaction energy, PIO analysis was performed for **15** and **15**$_{NMM}$ (Figure 8). Both TSs, **15** and **15**$_{NMM}$, share similar interaction modes: one d(Os) → σ*(N–O) interaction, one p(O) → σ*(Os–O) interaction and one p(O) → π*(Os–O) interaction. Although PIO analysis was performed for the TSs, the orbital's energies for a TS is in general affected by its position on the reaction coordinate, and it is more informative to consider the corresponding minimums. Localized orbitals of **11**$_{NMO}$ and **11**$_{NMO.NMM}$ shows a good consistency with the TSs, and the energy levels of the corresponding localized orbitals are shown in Figure 8. It is shown that the NMM ligand increases the energy level of d(Os), leading to a much stronger mixing with the antibonding σ*(N–O) orbital, in consistence with the longer N–O bond in **15**$_{NMM}$. The raise of the d-orbital energy could be attributed to the 4e-interaction of the ligand lone pair and metal occupied d-orbital. The mixing of p(O) to the O(trans)–Os antibonding orbital is also strengthened by the lowered σ*(Os–O) energy in the presence of NMM. Although some stabilizing effect is provided by the stronger orbital mixing, in consistence with the larger interaction term for **15**$_{NMM}$, its magnitude cannot compensate the resulted structural distortion, and the overall result is destabilization.

In summary, in this section we firstly explored the nature of the Os–NMO interaction in the reoxidation step, and then further discussed the reason why one extra NMM ligand significantly raises the barrier of reoxidation. The NMO molecule forms a covalent σ bonding with the Os center, and two different types of Os–O π bonding were developed synchronously along the oxo-transfer process. By combining distortion/interaction analysis and orbital analysis, we found that, although the presence of NMM leads to much stronger Os–NMO interaction, it cannot outcompete the unfavorable geometry distortion of both the Os part and the NMO fragment. Strong orbital interaction with σ*(N–O) results in a more dissociated N–O bond in the NMO fragment, and the collinear alignment of the O(trans)–Os with the forming Os–O multiple bonds in the hexacoordinated Os center of **15**$_{NMM}$ leads to strong trans-influence that weakens the trans-O–Os bonding. All these factors cause large energy compensation, and finally results in the high energy of **15**$_{NMM}$.

Mechanism of releasing the diol from Os(VI) bisglycolate 17 and completing the cycle. Pathways to release diol **9** from of Os(VI) bisglycolate **17** were investigated (Figure 9). Firstly, oxidation of **17** by NMO prior to hydrolysis can be excluded (see **5**→**7**, Figure 1); formation of Os(VIII) bisglycolate **17**$_{[ox]}$ is highly endergonic of 38.6 kcal/mol and so any possibility of having a third cycle is totally disallowed. Instead, stepwise hydrolytic release of diol **9** proceeds according to an associative pathway by way of octahedral intermediates **17**$_{H2O}$ and **31**$_{NMO}$ as an endergonic process of ΔG = 9.7 kcal/mol (Figure 9, right). Coordination of H_2O to **17** is endergonic of 7.8 kcal/mol to give **17**$_{H2O}$. Now, the dissociation of the glycolate ligand from the Os(VI) centre via four-membered ring TS **30** needs 16.5 kcal/mol, so an overall barrier of 24.3 kcal/mol is seen from **17** as an endergonic step of 13.9 kcal/mol to give **31**. Surprisingly, an overall higher barrier of 27.0 kcal/mol is found for hydrolysis by way of six-membered TS **30**$_{H2O}$, with an endergonicity of 17.9 kcal/mol to give **31**$_{H2O}$. In contrast to the first dissociation during glycolate opening, the glycolate dissociation shows modest

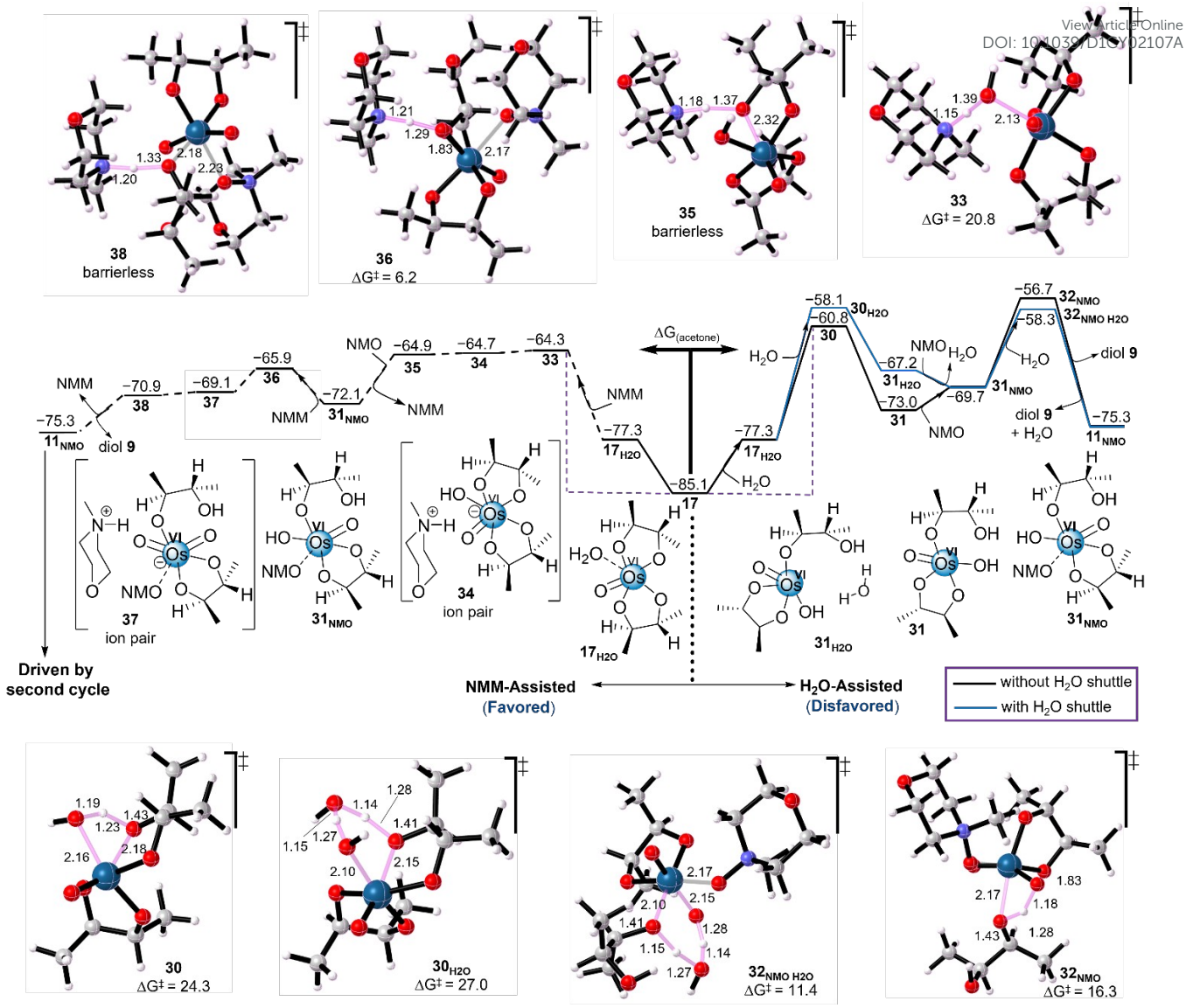

Fig. 9. Hydrolysis of bisglycolate Os(VI), with (left) and without (right) involvement of NMM, and disfavored reoxidation to dioxobisglycolate Os(VIII), calculated by the SMD-(acetone)-M06/6-311+G(d,p),def2-TZVP//M06/6-31G(d),LANL2DZ level of theory at 298.15 K. Bond lengths in angstrom and energies in kcal/mol

preference for six-membered TS **32**$_{NMO\ H2O}$ with a barrier of 11.4 kcal/mol as a slightly exergonic step to release the diol **9** and regenerate the NMO-complexed Os(VI) glycolate **11**$_{NMO}$, which can propagate the catalytic cycle. The high barriers and endergonicity are consistent with slow hydrolysis of Os(VI) bisglycolates under neutral conditions and the known stability of such intermediates isolated from dihydroxylation reactions using NMO.[16]

In addition to the hydrolysis promoted by water-shuttle, a stepwise NMM-assisted hydrolysis process was proven to be kinetically more favored (Figure 9, left). Starting from **17**$_{H2O}$, another water molecule adds to the Os center, accompanied by a proton transfer to an incoming NMM, giving an ion-pair intermediate **34** with an overall barrier of 20.8 kcal/mol via **33**, that means 13.0 kcal/mol from **17**$_{H2O}$. Then, the NMM-H$^+$ fragment protonates the alkoxyl group through a barrierless TS **35** giving **31**$_{NMO}$. The NMM-assisted hydrolysis of the second alkoxyl group in **31**$_{NMO}$ exhibits a reduced barrier of 6.2 kcal/mol via a similar stepwise proton transfer process, through TS **36**, ion pair **37** and TS **38**. This barrier is substantially lower than the water-shuttled pathway (TS **32**$_{NMO.H2O}$).

Inspection of the calculated energies for the steps leading to formation of diol **9** shows hydrolysis of oxobisglycolate Os(VI) **17** to be rate-determining in the second cycle pathway. Interestingly, we found tautomerization of hydrate **17**$_{H2O}$ to the dihydroxy complex **6** (Figure 1, R = Me) to be thermodynamically disfavoured (ΔG = 29.4 kcal/mol, see SI). Corresponding osmate dianion complexes have been isolated experimentally, but upon protonation, their free acids were found to rapidly return oxobisglycolates **17** rather than **6**.[16a]

View Article Online
DOI: 10.1039/D1CY02107A

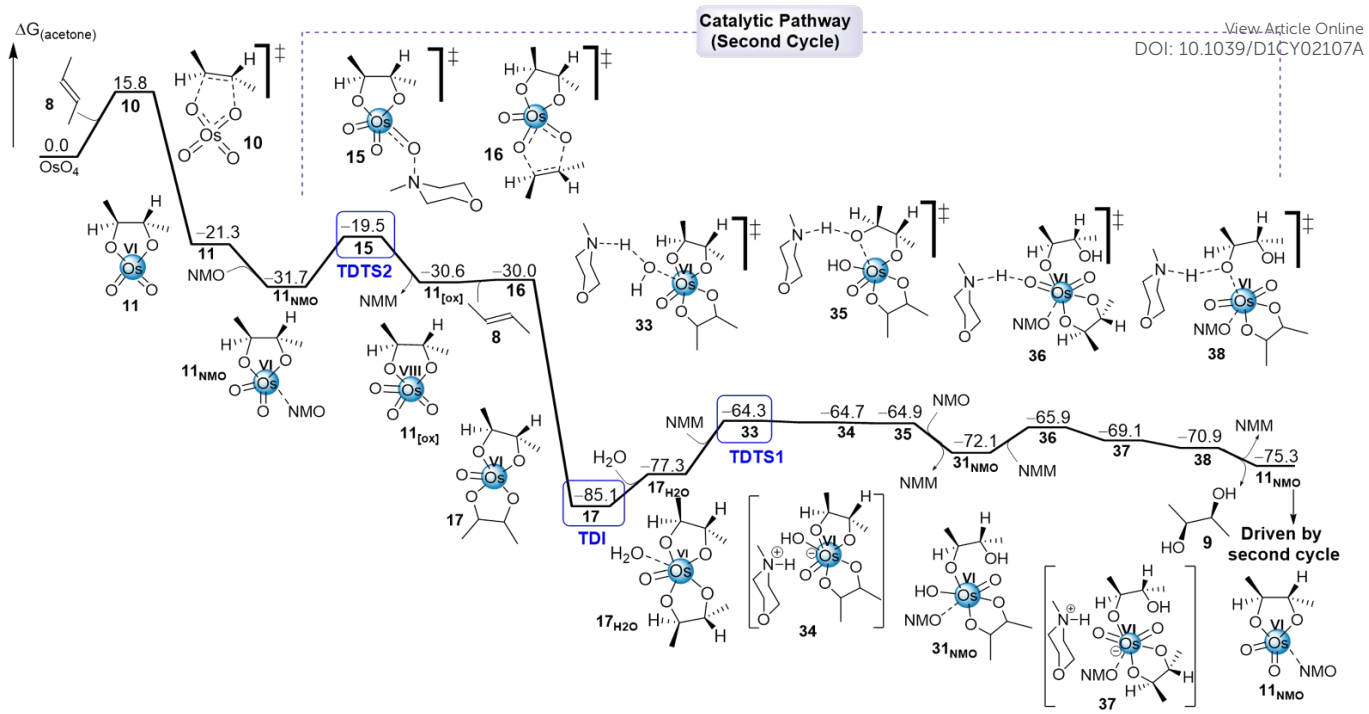

Fig. 10. Proposed reaction profile for dihydroxylation of alkenes under homogeneous conditions calculated at 298.15 K (in kcal/mol).

Proposed catalytic cycle and its efficiency. Based on the findings described above, a catalytic cycle for Upjohn dihydroxylation of a representative *trans*-disubstituted alkene under neutral conditions is presented (Figure 10). Os(VI) dioxoglycolate **11** is initially produced by (3+2) cycloaddition of OsO_4 and olefin **8**. Reoxidation of **11** proceeds via NMO complex Os(VI) glycolate $\mathbf{11_{NMO}}$ to give a reactive Os(VIII) trioxoglycolate $\mathbf{11_{[ox]}}$, which rapidly undergoes second cycle osmylation as a near-barrierless process and as a highly exergonic reaction ($\mathbf{11_{[ox]}}$→**17**). Hydrolysis of the resulting Os(VI) bisglycolate follows an associative pathway, releasing diol **9**, facilitated by NMM-assisted ion pair stepwise process with regeneration of the NMO-complexed Os(VI) dioxoglycolate to continue the catalytic cycle.

To evaluate the catalytic efficiency and its turnover frequency (TOF) in our theoretically obtained energy profile, the energetic span model proposed by Shaik and Kozuch [30] is used to determine the apparent free energy of activation for the entire proposed catalytic cycle. This model examines the compatibility of the resulting overall barrier with the experimental conditions. In this model, two fundamental terms are considered which are the TOF-determining transition state (TDTS) and the TOF-determining intermediate (TDI). The calculated catalytic cycle appeared in Fig. 10 shows two states of TDTS, hydrolysis (TDTS1) and reoxidation (TDTS2) steps, with one single TDI on the hydrolysis step. On one hand, the TDTS1 appears after the TDI, located on **17**, the energetic span 1 (δE1) is determined to be 20.8 kcal/mol, and so TOF1 = 12.67 h^{-1}. On the other hand, although the TDTS2 appears before the TDI, another energetic span δE2 has to be overcome to continue the catalytic cycle. Starting from **17** to **15** in the next catalytic cycle, the calculated energy is δE2 = 22.0 kcal/mol, since the ΔG_r = −43.6 kcal/mol, which is faster than δE1 and so TOF = 1.67 h^{-1}. According to these results, we conclude that the rate-determining state composes of reoxidation rather than hydrolysis step, and thus reoxidation is turnover-limiting state.[18]

Conclusion

The mechanism of catalytic non-enantioselective dihydroxylation of alkenes under homogenous conditions (OsO_4/NMO) has been explored using DFT calculations, finding the second cycle to be the preferred pathway. The Os(VI) glycolate **11**, generated by well-known osmylation of alkene substrate by OsO_4, is slow to undergo hydrolysis under either NMO-complexed Os(VI) or ligand-naked Os(VI) intermediates. Instead, this Os(VI) glycolate **11** is preferentially reoxidized by NMO to afford the Os(VIII) dioxoglycolate $\mathbf{11_{[ox]}}$ which then osmylates another alkene molecule to afford Os(VI) bisglycolate **17**, entering the so-called second cycle, rather than hydrolysis of Os(VIII) trioxoglycolate. Although amine ligands are known to catalyze alkene osmylation by OsO_4, the present study shows that tertiary amines like NMM do not promote either reoxidation or hydrolysis of Os(VI) glycolate but inhibit the reaction by competing coordination. The coordination of NMM to Os(VI) was found to be outpaced by coordination of NMO, where NMO binds stronger to Os(VI) than NMM, and subsequently reoxidation is favored under homogenous conditions to subsequently enter the second cycle.

The favorable interaction between NMO and Os(VI) and orbital nature of the reoxidation reaction in the presence and absence

View Article Online
DOI: 10.1039/D1CY02107A

of NMM have been rationalized. The NMO forms a covalent σ-bonding with the Os(VI) center in which two types of Os–O π-bonding are synchronously developed along the oxo-transfer process where Os center donates its d-electron to the σ*(N–O) orbital during interaction with NMO and accepts oxygen p-electron with both σ*(Os–trans-O) and π*(Os–O). Although addition of NMM strengthens the Os–NMO interaction in the oxo-transfer transition state, a competing unfavorable geometry distortion of both the Os part and the NMO fragment is seen due to the strong orbital interaction with σ*(N–O) that enhances a dissociated N–O bond and leads to an increased *trans*-influence of **15$_{NMM}$**. This *trans*-influence weakens the trans-O–Os glycolate bonding which subsequently causes a large unfavorable distortion energy that resulting in high barrier needed from **15$_{NMM}$** compared to **15** and confirming that reoxidation of Os(VI) glycolate is competing pathway even in the presence of tertiary amines.

The hydrolysis of Os(VI) bisglycolate **17** proceeds through an intermediate where the incoming water molecule coordinates with the Os center, and this hydrolysis proceeds via a stepwise ion-pairing facilitation assisted by the coproduct of reoxidation, NMM, to furnish the diol and regenerate the NMO-complexed Os(VI) intermediate to persist the catalytic cycle through only second cycle. Our computations showed that hydrolysis of **17** was determined to be highly slow when it is only water-assisted diol release. The results indicated that the amine-N-oxide, NMO, not only plays as an oxidant (Os(VI)→Os(VIII)), but also assists the hydrolysis of the stable Os(VI) bisglycolate **17** through the coproduct NMM released from reoxidation and by stabilizing the stepwise ion-pairing hydrolysis of **17** as a ligand (NMO). The so-common proposed intermediates Os(VIII) dioxo- and Os(VI) dihydroxy-bisglycolates (**17$_{[ox]}$** and **6**) were excluded as intermediates under neutral or homogenous conditions due to the energetic demand accompanying this process as a result of the disfavorable octahedral geometries required for either Os(VIII) dioxo- or Os(VI) dihydroxy-bisglycolates.

Using energetic span model for the proposed computed catalytic cycle, reoxidation (Os(VI)→Os(VIII) glycolate) was found to be turnover-limiting states.

This computational work offers new insights into important steps in Os-catalyzed dihydroxylation and helps inform future developments in asymmetric Os-catalyzed transformations.[31]

Computational Methods

All calculations were performed using Gaussian 09 program.[32] For geometry optimization, the hybrid meta-generalized gradient approximation functional M06 [33,34] was used with the LANL2DZ pseudopotential and basis set [35] for Os and 6-31G(d) basis set [36,37] for other atoms. All minimums were verified by the absence of negative eigenvalues in the vibrational frequency analysis. Transition state structures were found using the Berny algorithm [38] and verified by their imaginary frequency. Single point energies were calculated with the def2-TZVP basis set [39] for Os and 6-311+G(d,p) for others. Solvent effect of acetone was included via the SMD implicit solvation model [40] in the single point energy calculation. Intrinsic reaction coordinate (IRC) calculations were performed for the identified transition states to make sure they are correctly located.[41] Gibbs free energies were obtained through thermochemical corrections derived from vibrational frequencies at 298.15 K using unscaled frequencies and single point energies at the M06/6-311+G(d,p),def2-TZVP level of theory. All activation free energies are quoted relative to infinitely separated reagents. Optimized structures are illustrated using CYLview.[42] To take the effect of concentration in our computations, we used a concentration correction from standard state in gas phase, 1 atm, to standard state in solution, 1 mol/l at 298 K, so this conditional correction is responsible for the addition of 1.89 kcal/mol to the Gibbs energy of each calculated species involved in this study at 298 K. To understand the nature of interaction during the oxygen atom transfer, the analysis of bond order and localized orbital were employed to give new significant electronic insights.[43] In our work, totally 68 points were extracted from the IRC path of **15** and **15$_{NMM}$** and single point calculation at M06/6-31G(d),LANL2DZ level was run for each point. The contribution to the total bond order by a special bonding interaction is obtained by the following procedure: a) run a Pipek-Mezey orbital localization; b) calculate the total bond order between interested atoms (namely B.O.1); c) Manually find out the orbital interested based on the localized orbital, and set its occupation number to zero; d) Calculate the bond order based on the new density matrix (namely B.O.2); and e) then the contribution of this orbital to the total bond order is derived by B.O.1 minus B.O.2. The PIO analysis was performed using the open-source PIO program available at https://github.com/jxzhangcc/PIO.[28]

Author Contributions

The manuscript was written through the contributions of all authors. A.A.H. designed, conceived the study, and wrote and finalized the manuscript. Y.M. carried out DFT calculations and analyse and wrote the data and contribute to the discussions. G.A.I.M. contributed to the discussions and proofreads. All authors have given approval to the final version of the manuscript.

Conflicts of interest

There are no conflicts to declare

Acknowledgements

The authors acknowledge the computational resources the iridis4 supercomputers supported by the University of Southampton. A.A.H. highly acknowledges the University of Southampton/School of Chemistry for providing the scientific visiting (2717441/EB00-VISIT). A.A.H. thanks Prof. Richard C. D. Brown for his valuable proofread, discussions, and contributions to the early version of this work.

Notes and references

1 H. C. Kolb, M. S. Vannieuwenhze, and K. B. Sharpless, *Chem. Rev.* **1994,** 94, 2483-2547. (b) C. Nativi, S. Roelens,1,2-Diols. In *Science of Synthesis*; Clayden, J., Ed.; Thieme: Stuttgart, **2008**; Vol. 36, pp 757-774.

2 M. M. Heravi, V. Zadsirjan, M. Esfandyari, and T. B. Lashaki, *Tetrahedron: Asymmetry* **2017,** 28, 987-1043. (b) A. B. Zaitsev and H Adolfsson, *Synthesis* **2006**, 2006, 1725-1756. (c) I. E. Marko, and J. S. Svendsen, Dihydroxylation of carbon-carbon double bonds. In *Comprehensive Asymmetric Catalysis II*; E. N. Jacobsen, A. Pfaltz, and H. Yamamoto, Springer: Berlin, **1999**; pp 713-787.

3 For Os-free asymmetric *syn*-dihydroxylation see: (a) For Ru: C. J. R. Bataille, and T. J. Donohoe, *Chem. Soc. Rev.* **2011**, 40, 114–128. (b) For Mn: J. W. de Boer, W. R. Browne, S. R. Harutyunyan, L. Bini, T. D. Tiemersma-Wegman, P. L. Alsters, R. Hage, and B. L. Feringa, *Chem. Commun*. **2008**, 44, 3747–3749. (c) T. W.-S. Chow, Y. Liua , and C.-M. Che, *Chem. Commun*., **2011**, 47, 11204–11206. (d) R. A. Bhunnoo, Y. Hu, D. I. Lainé, and R. C. D. Brown, *Angew. Chem. Int. Ed.* **2002**, 41, 3479–3480. (e) C. Wang, L. Zong, and C.-H. Tan, *J. Am. Chem. Soc.* **2015**, 137, 10677–10682. (f) For Fe: K. Suzuki, P. D. Oldenburg, and L. Jr. Que, *Angew. Chem. Int. Ed.* **2008**, 47, 1887–1889. (g) C. Zang, Y. Liu, Z.-J. Xu, C.-W. Tse, X. Guan, J. Wei, J.-S. Huang, and C.-M. Che, *Angew. Chem. Int. Ed.* **2016**, 55, 10253–10257. (h) For bimetallic (Pd/Au): B. Hao, M. J. Gunaratna, M. Zhang, S. Weerasekara, S. N. Seiwald, V. T. Nguyen, A. Meier, and D. H. Hua, *J. Am. Chem. Soc.* **2016**, 138, 16839–16848. (i) For using Cyclic Diacyl Peroxide see: A. Pilevar, A. Hosseini, J. Becker, and P. R. Schreiner**,** *J. Org. Chem.* **2019**, 84, 12377−12386.

4 K. B. Sharpless, and K. Akashi, *J. Am. Chem. Soc.* **1976,** 98, 1986-1987.

5 Upjohn dihydroxylation: (a) W. P. Schneider, and A. V. McIntosh, Hydroxylation of $\Delta^{17(20)}$-Pregnenes. U.S. Patent 2,769,824, Nov. 6, **1956**. (b) V. Vanrheenen, R. C. Kelly, and D. Y. Cha, *Tetrahedron Lett.* **1976**, 1973-1976. (c) E. N. Jacobsen, I. Marko, W. S. Mungall, G. Schroder, and K. B Sharpless, *J. Am. Chem. Soc.* **1988,** 110, 1968-1970.

6 Racemic: (a) $K_3Fe(CN)_6/K_2CO_3$: M. Minato, K. Yamamoto, and J Tsuji, *J. Org. Chem.* **1990,** 55, 766-768. Asymmetric: (b) H. L. Kwong, C. Sorato, Y. Ogino, C. Hou, and K. B Sharpless, *Tetrahedron Lett.* **1990,** 31, 2999-3002.

7 For selected computational investigations of osmylation of alkenes by (3+2) and (2+2) pathways: (a) D. H. Ess, *J. Org. Chem.* **2009,** 74, 1498-1508. (b) X. Zhang, K. Wang, and R Fang, *Sci. China, Ser. B: Chem.* **2008**, 51, 19-24. (c) J. Frunzke, C. Loschen, and G. Frenking, *J. Am. Chem. Soc.* **2004,** 126, 3642-3652. (d) D. V. Deubel, and G. Frenking, *Accounts Chem. Res.* **2003,** 36, 645-651. (e) P.-O. Norrby, T. Rasmussen, J. Haller, T. Strassner, and K. N. Houk, *J. Am. Chem. Soc.* **1999,** 121, 10186-10192. (f) A. J. DelMonte, J. Haller, K. N. Houk, K. B. Sharpless, D. A. Singleton, T. Strassner, and A. A. Thomas, *J. Am. Chem. Soc.* **1997,** 119, 9907-9908. (g) J. Haller, T. Strassner, and K. N. Houk, *J. Am. Chem. Soc.* **1997,** 119, 8031-8034. (h) U. Pidun, C. Boehme, and G. Frenking, *Angew. Chem., Int. Ed.* **1996,** 35, 2817-2820. (i) S. Dapprich, G. Ujaque, F. Maseras, A. Lledos, D. G. Musaev, and K. Morokuma, *J. Am. Chem. Soc.* **1996,** 118, 11660-11661. For related computational studies of aminohydroxylation and diamination: (j) D. Munz, and T. Strassner, *J. Org. Chem.* **2010,** 75, 1491-1497. (k) D. V. Deubel, and K. Muniz, *Chem. Eur J.* **2004,** 10, 2475-2486.

8 J. S. M. Wai, I. Marko, J. S. Svendsen, M. G. Finn, E. N. Jacobsen, and K. B. Sharpless, *J. Am. Chem. Soc.* **1989,** 111, 1123-1125.

9 K. B. Sharpless, W. Amberg, Y. L. Bennani, G. A. Crispino, J. Hartung,; K. S. Jeong, H. L. Kwong, K. Morikawa, Z. M. Wang, D. Q. Xu, and X. L. Zhang, *J. Org. Chem.* **1992,** 57, 2768-2771.

10 P. Dupau, R. Epple, A. A. Thomas, V. V. Fokin, and K. B. Sharpless, *Adv. Synth. Catal.* **2002,** 344, 421-433.

11 M. R. Sivik, J. C. Gallucci, and L. A. Paquette, *J. Org. Chem.* **1990,** 55, 391-393.

12 (*E*)-But-2-ene was selected as a representative alkene in this work. Hydrolysis of Os glycolates are known to be slower for more sterically demanding alkenes.

13 The level of theory showed good agreement with experimental kinetic data for osmylation of alkenes, including (*E*)-but-2-ene. Please see Supporting Information of this reference: A. A. Hussein, M. J. S. Phipps, C. K. Skylaris, and R. C. D. Brown, *J. Org. Chem.* **2019**, 84, 15173-15183.

14 Calculations are performed on low spin configurations, which is consistent with reported electronic configurations of Os(VIII) and Os(VI) oxoglycolates. (a) L. R. Subbaraman, J. Subbaraman, and E. J. Behrman, *Inorg. Chem.* **1972,** 11, 2621-2627. (b) R. J. Collin, J. Jones, and W. P. Griffith, *J. Chem. Soc., Dalton Trans.* **1974**, 1094-1097.

15 Calculated activation energy for osmylation is in good agreement with reported experimental values (a) D. W. Nelson, A. Gypser, P. T. Ho, H. C. Kolb, T. Kondo, H. L. Kwong, D. V. McGrath, A. E. Rubin, P.-O. Norrby, K. P. Gable, and K. B. Sharpless, *J. Am. Chem. Soc.* **1997,** 119, 1840-1858. (b) H. C. Kolb, P. G. Andersson, Y. L. Bennani, G. A. Crispino, K. S. Jeong, H. L. Kwong, and K. B. Sharpless, *J. Am. Chem. Soc.* **1993,** 115, 12226-12227. (c) P. G. Andersson, and K. B. Sharpless, *J. Am. Chem. Soc.* **1993,** 115, 7047-7048.

16 Os(VI) oxobisglycolates have been prepared by complexation of 1,2-diols to $K_2[OsO_2(OH)_4]$. (a) R. Criegee, B. Marchand, and H. Wannowius, *Leibigs Ann. Chem.* **1942**, 550, 99-133. (b) M. Schroeder, *Chem. Rev*. **1980**, *80*, 187-213.

17 A. A. Hussein, *RSC Advances*, **2020**, 10, 15228−15238. (b) A. L. Tenderholt, K. O. Hodgson, B. Hedman, R. H. Holm, and E. I. Solomon, *Inorg. Chem.* **2012,** 51, 3436-3442.

18 E. N. Jacobsen, I. Marko, M. B. France, J. S. Svendsen, and K. B. Sharpless, J. Am. Chem. Soc. **1989**, 111, 739-740.

19 OsO_4•NMO was isolated by Bailey *et al.* (see ref 18) as a labile complex, supporting weak complexation of the *N*-oxide ligand to OsO_4 (ΔG = −1.6 kcal/mol, see ref 12).

20 A. J. Bailey, M. G. Bhowon, W. P. Griffith, A. G. F. Shoair, A. J. P. White, and D. J. Williams, *J. Chem. Soc., Dalton Trans.* **1997**, 3245-3250.

21 For experimental studies of the reoxidation kinetics for Os(VI) to Os(VIII), which have identified reoxidation by NMO to be rate determining under Upjohn conditions: (a) E. Erdik, and D. Kahya, *J. Phys. Org Chem.* **2002,** 15, 229-232. (b) E. Erdik, D. Kahya, and T. Daskapan, *Synth. Commun.* **1998,** 28, 1-7. (c) E. Erdik, and D. Kahya, *Int. J. Chem. Kinet.* **1997,** 29, 359-366. (d) E. Erdik, and D. S. Matteson, *J. Org. Chem.* **1989, 54**, 2742-2748.

22 For X-ray structures showing distorted square-pyramidal Os(VI) oxobisglycolates: ref. 10 and (a) R. Collin, W. P. Griffith, F. L. Phillips, and A. C. Skapski, *Biochim. Biophys. Acta* **1973,** 320, 745-747. (b) A. Lehtonen, J. Jokela, P. G. Edwards, and R. Sillanpaa, *J. Chem. Soc., Dalton Trans.* **1999**, 2785-2788. For other characterization: (c) D. V. Mcgrath, G. D. Brabson, and K. B. Sharpless, L. Andrews, *Inorg. Chem.* **1993,** 32, 4164-4165.

23 L. G. Marzilli, B. E. Hanson, T. J. Kistenmacher, L. A. Epps, R. C. Stewart, Inorg. Chem. **1976**, *15*, 1661–1665.

24 S. Díaz-Moreno, D. T. Bowron, *Organometallics* **2003,** 22*,* 390-394.

25 A. Mayer, *Chem. Phys. Lett.* **1983,** 97*,* 270-274.

26 J. Pipek, and P. G. Mezey, *J. Chem. Phys.* **1989,** 90*,* 4916-4926.

27 F. M. Bickelhaupt, and K. N. Houk, *Angew. Chem. Int. Ed.* **2017,** 56, 10070-10086.

View Article Online
DOI: 10.1039/D1CY02107A

28 (a) J.-X. Zhang, F. K. Sheong, and Z. Lin, *WIREs Comput. Mol. Sci.* **2020,** 10, e1469. (b) J.-X. Zhang, F. K. Sheong, and Z. Lin, *Chem. Eur. J.* **2018,** 24, 9639-9650.
29 T. G. Appleton, H. C. Clark, and L. E. Manzer, *Coord. Chem. Rev.* **1973**, 10, 335-422.
30 (a) Kozuch, Wiley Interdiscip. *Rev. Comput. Mol. Sci*, **2012**, *2*, 795-815. (b) S. Kozuch, and S. Shaik, *Acc. Chem. Res*. **2011**, 44, 101–110.
31 For recent on 1,2-difuntionalization of alkenes see: For enantioselective Pd diacetoxylation of alkenes (a) B. Tian, P. Chen, X. Leng, and G. Liu, *Nat. Catal.* **2021**, 4**,** 172-179. For electrophotocatalytic acetoxyhydroxylation of olefines (b) H. Huang, and T. H. Lambert, *J. Am. Chem. Soc.* **2021,** 143, 7247-7252.
32 M. J. Frisch, *et al*. *Gaussian 09*, Gaussian, Inc.: Wallingford, CT, USA, **2009**.
33 Y. Zhao, and D. G. Truhlar, *Chem. Phys. Lett.* **2011,** 502, 1-13.
34 Y. Zhao, and D. G. Truhlar, *Theor. Chem. Acc.* **2008,** 120, 215-241.
35 P. J. Hay, and W. R. Wadt, *J. Chem. Phys.* **1985,** 82*,* 270-283.
36 P. C. Hariharan, and J. A. People, *Theor. Chem. Acc.* **1973,** 28, 213-222.
37 W. J. Hehre, R. Ditchfield, and J. A. People, *J. Chem. Phys.* **1972,** 56*,* 2257-2261.
38 (a) H. B. Schlegel, *J. Comput. Chem.* **1982,** 3, 214-218. (b) X. S. Li, and M. J. Frisch, *J. Chem. Theory Comput.* **2006,** 2, 835-839.
39 F. Weigend, and R. Ahlrichs, *Phys. Chem. Chem. Phys.* **2005,** 7*,* 3297-3305.
40 V. Marenich, C. J. Cramer, and D. G. Truhlar, *J. Phys. Chem. B.* **2009,** 113, 6378-6396.
41 (a) K. Fukui, *Acc. Chem. Res*. **1981**, *14*, 363-368. (b) H. P. Hratchian, and H. B. Schlegel, *J. Chem. Phys.* **2004**, 120, 9918-9924. (c) H. P. Hratchin, and H. B. Schlegel, *J. Chem. Theory and Comput.*, **2005**, 1, 61-69.
42 (a) C. Y. Legault, 1.0b, *Université de Sherbrooke: Canada*, **2009** (http://www.cylview.org).
43 T. Lu, and F. Chen, *J. Comput. Chem.* **2012,** 33*,* 580-592